Materials Science and Technology, 2017
http://dx.doi.org/10.1080/02670836.2016.1258157

Effect of manganese sulphide particle shape on the pinning of grain boundary

L. Guo[a,*], H. Roelofs[b], M. I. Lembke[c], H. K. D. H. Bhadeshia[a]

[a]*Department of Materials Science and Metallurgy, University of Cambridge, 27 Charles Babbage Road, Cambridge CB3 0FS, U.K.*
[b]*R& D, Swiss Steel AG, Emmenweidstr. 90, CH-6020 Emmenbrücke, Switzerland*
[c]*Steeltec AG, Emmenweidstr. 72, CH-6020 Emmenbrücke, Switzerland*

Abstract

The pinning of austenite grain boundaries by manganese sulphide particles is examined experimentally as a function of the shape and size of the inclusions in a free-machining steel. With the same volume fraction, large and extremely long MnS particles are found to be more effective at hindering the motion of austenite grain boundaries than those that approximate spherical shape, even when the latter are smaller and have a higher number density.

Keywords: Zener drag, MnS, Grain boundary, Austenite, Free-machining steel

1. Introduction

Free-machining steels often are designed to contain a number of manganese sulphide inclusions. Their role in improving machinability is complex, but in simple terms, they influence the adhesion of the steel to the tool and enable chip-breaking [1, 2]. However, their presence has other consequences, for example in the development of the austenite grain structure and hence its subsequent transformation characteristics.

The effect of inclusions on grain growth, i.e. on grain boundary motion, was described by Smith [3] who argued that small particles could hinder the motion and that it did not require the formation of continuous boundary-films of some phase to immobilise the boundaries. Zener provided Smith with an estimate of the restraining effect of a spherical particle on a grain boundary [4], so the interaction of particles with boundaries has since then been referred to as Zener drag. The assumption of a spherical inclusion shape is common [3, 5–7], but in some cases a consideration of anisotropic shapes becomes important. Nes and co-workers [8] studied the pinning of grain boundaries by ellipsoidal particles oriented normal to the boundaries to find that particle shape and distribution are important factors in Zener drag. This orientation assumption was further relaxed by Li and Easterling who studied ellipsoidal particles with different axial ratios and orientations with respect to the grain boundary [9]. They concluded that an elongated particle is particularly effective when the long axis

*Corresponding author
Email address: lg446@cam.ac.uk,lei-guo@outlook.com (L. Guo)

is oriented parallel to the grain boundary with a dependence on the exact particle shape. However, these studies are mostly theoretical [8–12] with sparse experimental evidence.

In high sulphur free-machining steels, the MnS particles are usually quite large and very long in hot rolled bars, a few micrometres in diameter and length ranging from a few micrometres to millimetres. The purpose of the work presented here was to reveal the role of the particles in determining the austenite grain structure in the context of other work focused on predicting the transformation characteristics of such alloys [13–15].

2. Experimental details

A commercial free-machining steel in the hot-rolled condition was supplied by Swiss Steel AG in the form of rods 32 mm in diameter, with the chemical composition as listed in Table 1.

Test samples of 8 mm in diameter and 10 mm in length were prepared from the hot-rolled bar. One group of these samples was from a bar "homogenised" at 1200 °C for 48 h in a vacuum furnace, for comparison against the remaining samples that were left in the manufactured condition. All subsequent heat treatments were carried out in a THERMECMASTOR-Z thermomechanical simulator with a vacuum of around 10^{-3} Pa. To facilitate a clear characterisation of the austenite grain size, the cylindrical samples had flats polished along their lengths, by standard metallographic polishing method which was finished with 1 μm diamond paste, so that any thermal grooving at the austenite grain boundaries can be used to measure the grain size; the details are described in Ref. [16]. Three images from different locations were used to measure the grain size.

Synchrotron X-ray diffraction was used to examine the presence of any other precipitates or inclusions in the steel, the diffraction patterns from 3 mm diameter rod samples were collected by a Perkin Elmer XRD 1621 flat panel detector in the Deutsches Elektronen-Synchrotron (DESY) P07 beamline, with beam energy of 100 keV, spot size of 1 mm×1 mm and sample to detector distance of 1.280 m.

Table 1: Chemical composition (wt%) of the studied steel

C	Si	Mn	Ni	Mo	Cr	Cu	N	S	Al
0.22	0.97	1.53	0.18	0.14	1.54	0.17	0.0104	0.14	0.0042

3. Result and discussion

The austenite grain size as defined by the mean lineal intercept $\overline{L}_\gamma$, was naturally much greater following the homogenisation treatment when compared with the as-received state. To introduce a uniform and comparable γ-grain size and same microstructure, the temperature dependence of grain size needs to be investigated first. So samples were heated up to austenitisation temperatures of 1000 °C, 1100 °C or 1200 °C at a rate of 5 °C s^{-1}, holding for 5 min, followed by natural cooling inside the vacuum chamber to ambient temperature. The resulting austenite grain size as a function of austenitisation temperature is shown in Fig. 1. The reaustenitisation at 1085 °C for 5 min of the homogenised sample led to approximately

the same austenite grain size as the as-received sample reaustenitised at 1200 °C for 5 min, with $\overline{L}_\gamma = 50 \pm 3$ µm. So a pre-treatment to obtain the same starting austenite grain size and microstructure was carried out, i.e., austenitisation at 1085 °C for 5 min for the homogenised group, and at 1200 °C for 5 min for the as-received group, respectively, followed by cooling to ambient temperature. The samples with the same grain size were once again reaustenitised at 1000 °C, 1100 °C or 1200 °C for 5 min, respectively. Their austenite grain sizes were measured and are presented in Fig. 2. The size $\overline{L}_\gamma$ of the homogenised sample remained significantly greater than the as-received ones.

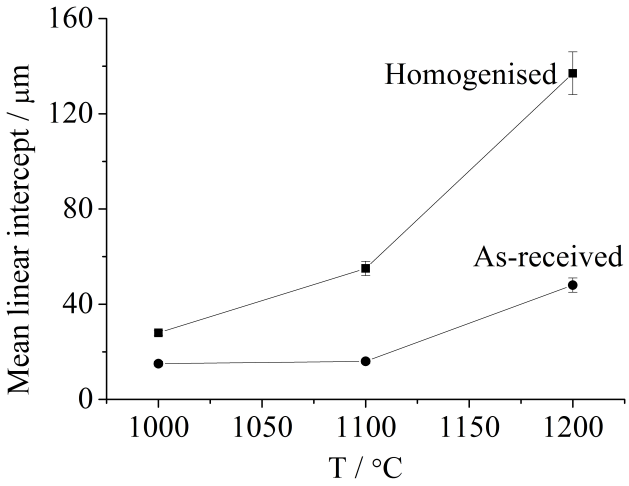

Figure 1: Austenite grain size as a function of reaustenitisation temperature for two groups of samples with different starting microstructure and austenite grain size, which is used to obtain the pre-treatment temperature.

Materials Science and Technology, 2017
http://dx.doi.org/10.1080/02670836.2016.1258157

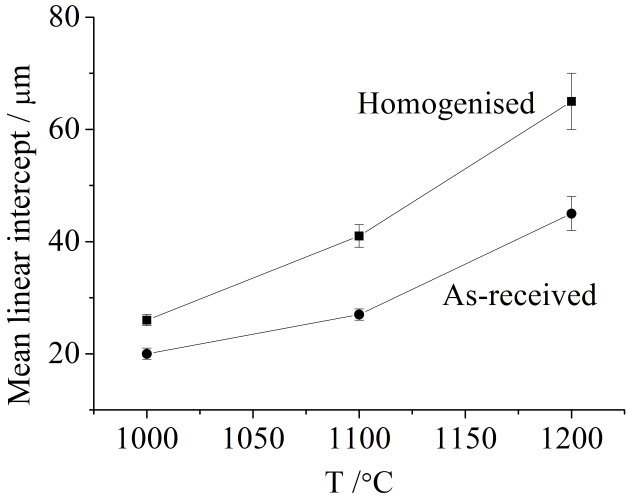

Figure 2: Austenite grain size as a function of reaustenitisation temperature for pre-treated samples with the same starting microstructure and austenite grain size. As-received samples were reaustenitised at 1200 °C for 5 min cooled to room temperature (RT), and reaustenitised once again at 1000 °C, 1100 °C or 1200 °C for 5 min, while the homogenised samples were reaustenitised at 1085 °C for 5 min cooled to ambient temperature, and reaustenitised again at 1000 °C, 1100 °C or 1200 °C for 5 min.

Equilibrium precipitates

Fig. 3 shows the calculated equilibrium phase fractions as a function of temperature using MatCalc version 5.52 with mc_fe_v2.000 database [17]; the phases allowed to exist were liquid, FCC_A1, BCC_A2, Cr_3Mn_5, Laves phase, cementite, Ksi carbide, M_6C, M_7C_3, $M_{23}C_6$, AlN, Fe_4N, FeS_2 and FeS_P. There are MnS, AlN, M_7C_3 and Laves phases that can in principle precipitate. MnS forms from liquid at about 1480 °C, it has a volume fraction of about 5×10^{-3} below 1440 °C. AlN starts to form at about 1060 °C and reaches a maximum fraction of 8×10^{-4} at 700 °C. M_7C_3 precipitates at 750 °C, and has a volume fraction of 3.5×10^{-2} below 700 °C. Laves phase starts to form at 530 °C, and has a volume fraction of 2×10^{-3} below 400 °C. The steel clearly is not at equilibrium since only MnS was detected as the precipitate phase using high energy synchrotron X-ray diffraction at room temperature, Fig. 4.

According to the calculations, only MnS and AlN should be present at the austenitisation temperatures of 1000 °C to 1200 °C. Aluminium nitride can hinder austenite grain growth [16, 18, 19]. The homogenisation treatment may lead to the dissolution of the AlN, which might explain why after homogenisation and reaustenitisation, $\overline{L}_\gamma$ remains greater than that of the samples reaustenitised from the as-received condition. In other words, the re-precipitation of AlN in a manner reduces Zener drag. Previous work using synchrotron X-rays clearly revealed the AlN [16], so the same method was applied to the present steel. Fig. 4 shows that AlN could not be detected in the as-received steel, consistent with the very low concentrations present. There are no other low intensity peaks except those of MnS, which are indicated by the blue arrows. Another explanation of the data in Fig. 2 is that homogenisation causes the large MnS particles to grow at the expense of smaller ones by Ostwald ripening, but in fact, the number density of particles increases as elongated sulphides split into arrays of smaller particles (Fig. 6). The real reason for the discrepancies following reaustenitisation of the

homogenised and as-received samples may therefore be associated with the different shapes of MnS particles in the two groups of specimens.

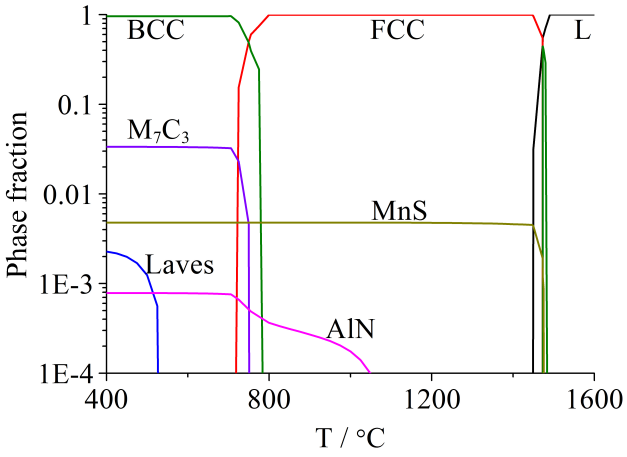

Figure 3: Equilibrium phase fraction of the alloy calculated by MatCalc. (L: Liquid, BCC:Ferrite, FCC: Austenite)

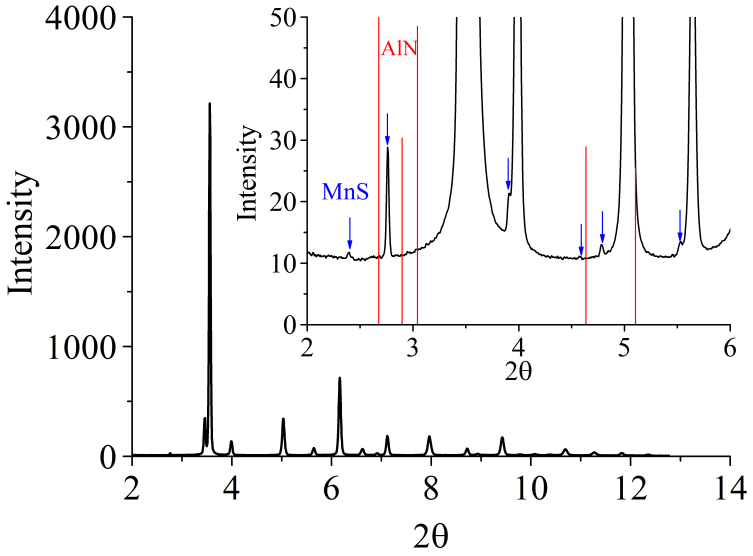

Figure 4: Synchrotron X-ray diffraction pattern of the as-received steel. The inset is a magnified portion of the spectrum where AlN major peaks should be with the five strongest peaks of AlN superimposed on, the heights of the five peaks are proportional to their theoretical intensities. The blue arrows indicating peak positions of MnS.

The MnS particles precipitate from liquid during solidification, as the samples were from hot rolled bar, most of the MnS particles are approximately circular in the transverse direction, shown in Fig. 5; while in the rolling direction, they are elongated by hot rolling, see Fig. 6 a, so they can be simplified to rods in three dimension for the as-received samples. Homogenisation broke down the elongated MnS particles into smaller ones in a manner akin

to the instabilities that occur in fluid streams, and induced some spheroidisation, as shown in Fig. 6 b.

Average sizes of the particles are $11.7 \pm 13.5\,\mu m^2$ (the uncertainty here is the standard deviation) for the as-received group and $6.6 \pm 10.0\,\mu m^2$ for the homogenised group, respectively. This may suggest that on average one particle broke into two, small short ones might not split at all, while large long particles divided into many particles. The average aspect ratio of the as received group is 6.2 ± 3.3, while that of the homogenised is 1.8 ± 0.8, hence partially spheroidised after homogenisation, aspect ratio of a sphere is 1.

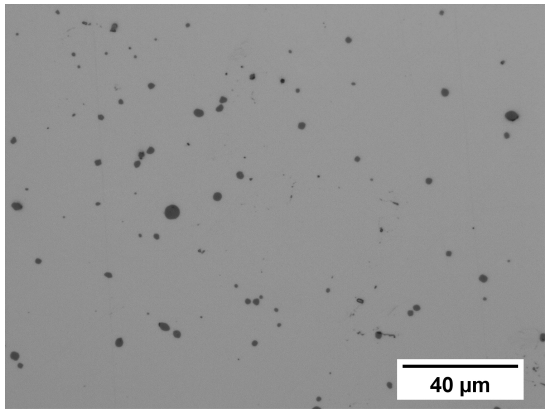

Figure 5: MnS particles on the transverse direction of the as-received sample.

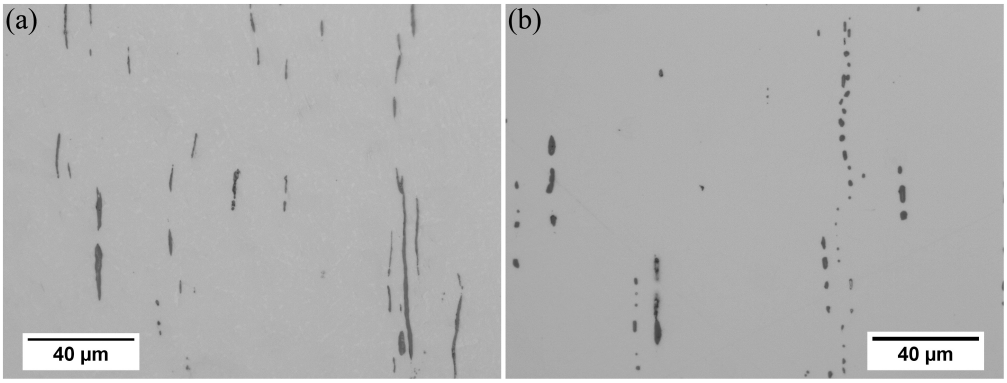

Figure 6: (a) MnS particles in the rolling direction of the as-received sample. (b) Fragmented MnS particles in the rolling direction after homogenisation at 1200 °C for 48 h.

MnS shape effect on pinning

The resistance from a particle on the motion of grain boundary is proportional to the length of the intersection line. When the grain boundary moves towards a spherical particle, there is a energy barrier for the boundary to contact the particle due to the creation of the intersection triple line [20]. This energy barrier is significant if the particle size is small, Zhao *et al* estimated that when the particle size is below 40 nm in Cu, the effect of the triple line tension is substantial [20]. But in the case of MnS particles whose sizes are a few micrometres, this effect may be neglected, so the classical approach is adopted, i.e. the triple line tension

is not considered. After the boundary overcomes the energy barrier it will be attracted to the particle, due to the need to balance the interfacial tensions and accompanying elimination of some boundary area. It is only when the boundary has passed the maximum radius and attempts to move away from the particle, that a drag force is exerted to hold it back. The maximum pinning force F_s due to a single spherical particle is given by

$$F_s = \pi r_s \sigma \tag{1}$$

where r_s is the radius of the particle and σ is the grain boundary energy per unit area.

For the rod-shaped MnS particle, when the particle is very long compared to the austenite grain, the segment of grain boundary which is in contact with the particle is held by the particle, as shown in Fig. 7, which means the rod lies in the plane of the boundary as illustrated in Fig. 8.

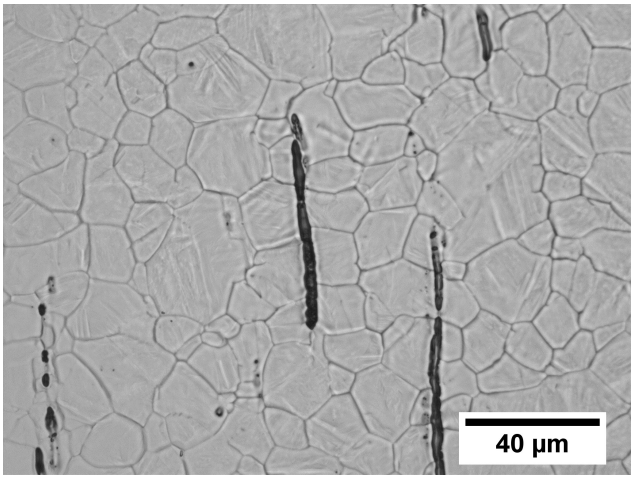

Figure 7: Large long particles hindering sideways grain growth.

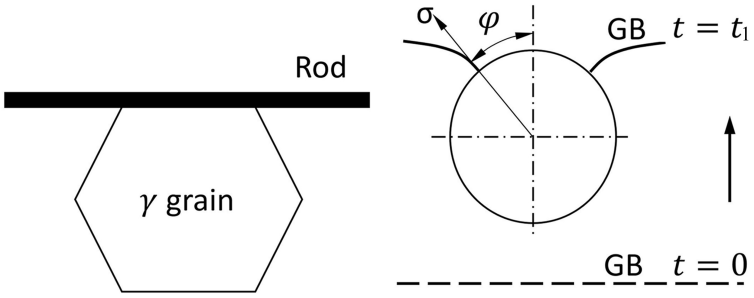

Figure 8: Schematic illustration of interaction between a long particle and an austenite grain boundary, with the parameters used in the model, GB: austenite grain boundary.

The pinning force produced by this rod particle is

$$F_{\text{rod}} = 2\sigma l_{\text{rod}} \cos\varphi = 4\sigma r_{\text{rod}} a \cos\varphi \tag{2}$$

where φ is the angle illustrated in Fig. 8, l_{rod} is the length of the rod, r_{rod} is the radius of the rod and $a = \frac{l_{\mathrm{rod}}}{2r_{\mathrm{rod}}}$ is the aspect ratio of the rod. The maximum drag force is

$$F_{\mathrm{rod}} = 4\sigma r_{\mathrm{rod}} a \tag{3}$$

The radius of a sphere with equal volume is $r_{\mathrm{s}} = \left(\frac{3}{2}a\right)^{\frac{1}{3}} r_{\mathrm{rod}}$, so the drag force of a spherical particle with equivalent volume is given by

$$F_{\mathrm{s}} = 2\pi\sigma r_{\mathrm{s}} \sin\varphi\cos\varphi = 2\pi\sigma r_{\mathrm{rod}} \left(\frac{3}{2}a\right)^{\frac{1}{3}} \sin\varphi\cos\varphi \tag{4}$$

with the maximum drag force given by

$$F_{\mathrm{s}} = \pi\sigma r_{\mathrm{rod}} \left(\frac{3}{2}a\right)^{\frac{1}{3}} \tag{5}$$

Therefore, the ratio of maximum drag force of a rod over that of the sphere of identical volume is

$$\frac{F_{\mathrm{rod}}}{F_{\mathrm{s}}} = \frac{4}{\pi}\left(\frac{2}{3}\right)^{\frac{1}{3}} a^{\frac{2}{3}} \tag{6}$$

If the rod now breaks into n identical spherical particles spread evenly in the same length of the rod, the radius of each sphere is $r'_{\mathrm{s}} = \sqrt[3]{3a/2n} \times r_{\mathrm{rod}}$, the ratio of the drag force of a rod over the total drag force of the n spherical particles is

$$\frac{F_{\mathrm{rod}}}{F'_{\mathrm{s}}} = \frac{4}{\pi}\left(\frac{2}{3}\right)^{\frac{1}{3}} \left(\frac{a}{n}\right)^{\frac{2}{3}} \tag{7}$$

The calculated ratio of pinning force of a long rod over n spheres whose total volume is the same as the rod is shown in Fig. 9. The ratio of maximum pinning force of a rod over the n spheres increases with the increase of aspect ratio, but decreases with an increase of n. For the average aspect ratio of 6 of the MnS particles found in this steel, if one rod particle breaks into 7 identical spheres spread evenly along the length of the rod, the pinning force of the rod is still larger than that of all the 7 spheres combined. Furthermore, a string of particles can be overcome by the the motion of grain boundary segments one by one, in contrast to the big elongated particles that cannot be passed by the grain boundary in that fashion, so the calculations above may be conservative in representing the efficacy of the rod-shaped sulphide. In current experiment, it was found that one MnS particle split into two on average after homogenisation, so the pinning force should be larger for the rod-shaped particle.

Li and Easterling found ellipsoid particle is more effective than a sphere of the same volume when its long axis is parallel to the grain boundary [9], which is the same orientation presented in this study. Fig. 10 shows the ratios of maximum pinning force of a rod and an ellipsoid over the equivalent sphere. Rod is slightly more effective than ellipsoid, the difference increases with aspect ratio which maybe attributed to the size of particles. In this study, the rod is assumed to be very long, spanning several austenite grains, so the effect of grain boundaries climb over the ends of the rod is neglected, while in their work the particle is

assumed to be small, hence boundaries overcome the ellipsoid from the ends as well, therefore reduces the efficiency.

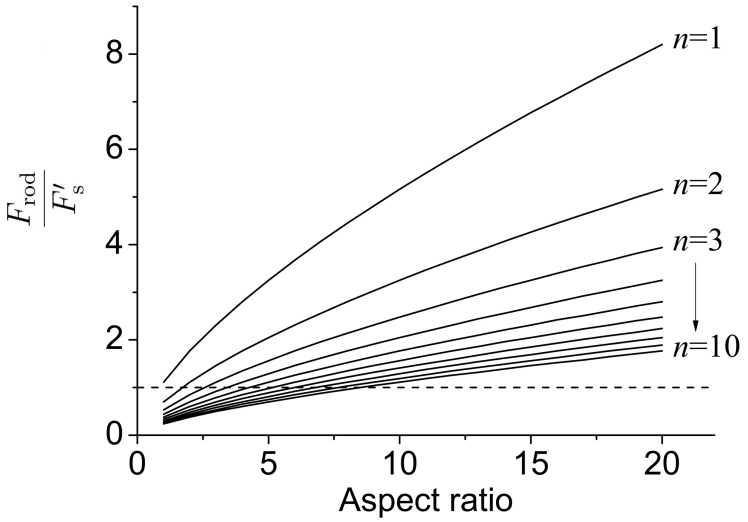

Figure 9: Calculated ratio of maximum drag force of a rod particle over n spherical ones with the same total volume. The horizontal dashed line indicate the equal pinning force.

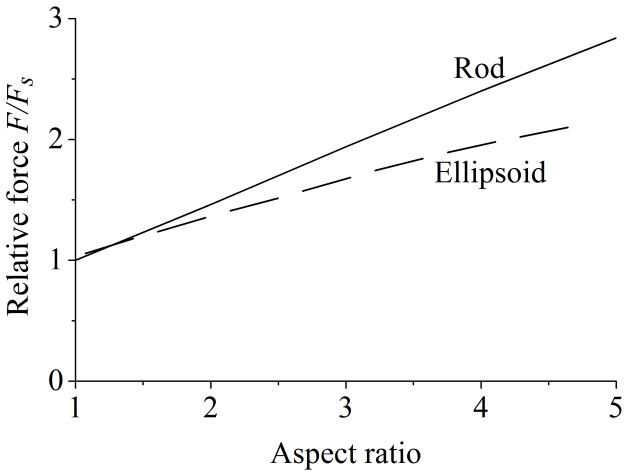

Figure 10: Comparison of the calculated ratio of maximum force of a rod and an ellipsoid over a sphere of equivalent volume. Ellipsoid data from Li and Easterling [9].

For the same volume fraction and number density of particles, different shapes can also change the probability of a particle intersecting a grain boundary. As the surface which is not facing the moving boundary induces a drag force, half of the precipitate surfaces will drag the boundary, and as the net interaction area increases so does the drag force. As the total precipitate surface area is depending on its shape, sphere has the smallest surface area per unit volume, so it should be the least effective, which is in agreement with the work of Ringer et al. [10], who found cubic particles to be more effective than spherical ones,

and more recently, Chang et al. [11] found needle-shaped particle to be more effective than spherical ones, and that the orientation of the needles in the sample had a small effect on pinning.

4. Conclusions

In summary, high-sulphur free-machining steels contain manganese sulphides, some of which are rod-shaped with lengths that span many austenite grains. The rods can be induced to break up into arrays of spherical particles by heat treatment at elevated temperatures, a process presumably driven by the minimisation of total interfacial energy. However, unlike coarsening reactions where the same driving force operates, the number density of particles increases due to the fragmentation of the rods into spheres.

The ratio of the Zener drag force due to long rod-shaped particles, to that of a series of n spheres that result from the fragmentation of a rod, is proportional to $\sqrt[\frac{2}{3}]{a/n}$, where a is the rod aspect-ratio. It follows that there are circumstances in which the influence of rods can be greater or less than that of spheres, as illustrated in Fig 9. This could be a general phenomenon if the second phase particles are long enough to span a few grains.

For the steel studied here, an elevated temperature 'homogenisation' heat treatment leads to an irreversible change in MnS morphology and number density. The effect is to reduce the Zener drag force so that the austenite grain size obtained during reaustenitisation following this homogenisation is always greater than the case where the homogenisation heat treatment is omitted.

Acknowledgement

The authors are grateful to Swiss Steel AG for funding this work and Professor M.G. Blamire for the provision of laboratory facilities at University of Cambridge.

References

[1] M. Merchant, N. Zlatin, Basic reasons for good machinability of free machining steels, Transactions of the American Society for Metals 41 (1949) 647–677.

[2] H. Yaguchi, Scanning electron microscopy and electron microprobe analysis of built-up edges in low carbon resulfurized free-machining steel, Materials Science & Engineering (1986) L27–L30.

[3] C. S. Smith, Grains, phases, and interfaces: An interpretation of microstructure, Transactions of the American Institute of Mining, Metallurgical, and Petroleum Engineers 175 (1948) 15.

[4] M. Hillert, Zener's pinning effect: role of dispersed particle on grain size, Tech. Rep. TRITA-MAC-0369, Royal Institute of Technology, Stockholm, Sweden (1988).

[5] P. Manohar, M. Ferry, T. Chandra, Five decades of the zener equation, ISIJ international 38 (1998) 913–924.

[6] B.-N. Kim, T. Kishi, Finite element simulation of zener pinning behavior, Acta materialia 47 (1999) 2293–2301.

[7] G. Gottstein, L. Shvindlerman, On the retardation of grain boundary motion by small particles, Scripta Materialia 63 (2010) 1089–1091.

[8] E. Nes, N. Ryum, O. Hunderi, On the zener drag, Acta Metallurgica 33 (1985) 11–22.

[9] W. B. Li, K. E. Easterling, The influence of particle shape on Zener drag, Acta Metallurgica et Materialia 38 (1990) 1045–1052.

[10] S. Ringer, W. Li, K. Easterling, On the interaction and pinning of grain boundaries by cubic shaped precipitate particles, Acta Metallurgica 37 (1989) 831–841.

[11] K. Chang, W. Feng, L.-Q. Chen, Effect of second-phase particle morphology on grain growth kinetics, Acta Materialia 57 (2009) 5229–5236.

[12] K. Chang, L.-Q. Chen, Quantitative evaluation of particle pinning force on a grain boundary using the phase-field method, Modelling and Simulation in Materials Science and Engineering 20 (2012) 055004.

[13] J. Chen, H. K. D. H. Bhadeshia, S. Hasler, H. Roelofs, U. Ulrau, Complete calculation of steel microstructure for strong alloys, in: T. Pérez (Ed.), New Developments on Metallurgy and Applications of High Strength Steels, Buenos Aires, TMS-AIME, Materials Park, Ohio, USA, 2008, pp. 749–759.

[14] H. Roelofs, S. Hasler, L. Chabbi, U. Urlau, J. Chen, H. K. D. H. Bhadeshia, Multiphase structures in case hardening steels following continuous cooling, in: T. Perez (Ed.), New Developments on Metallurgy and Applications of High Strength Steels,, TMS-AIME, Materials Park, Ohio, USA, 2008, pp. 761–768.

[15] L. Guo, H. Roelofs, M. Lembke, H. Bhadeshia, Modelling of transition from upper to lower bainite in multi-component system, Materials Science and Technology 0 (0) (0) 1–8. doi:10.1080/02670836.2016.1221495.

[16] H. Pous-Romero, I. Lonardelli, D. Cogswell, H. K. D. H. Bhadeshia, Austenite grain growth in a nuclear pressure vessel steel, Materials Science & Engineering A 567 (2013) 72–79.

[17] E. Kozeschnik, B. Buchmayr, Matcalc- a simulation tool for multicomponent thermodynamics, diffusion and phase transformations, in: Fifth International Seminar on the Numerical Analysis of Weldability, 1999, pp. 349–361.

[18] T. Gladman, F. B. Pickering, Grain coarsening of austenite, Journal of the Iron and Steel Institute 205 (1967) 653–664.

[19] M. Militzer, A. Gumelli, E. B. Hawbolt, T. R. Meadowcroft, Austenite grain growth kinetics in Al-killed plain carbon steels, Metallurgical and Materials Transactions A 27A (1996) 3399–3496.

[20] B. Zhao, G. Gottstein, L. Shvindlerman, Triple junction effects in solids, Acta Materialia 59 (9) (2011) 3510–3518.